Biochemistry

Open Access
This article is licensed under CC-BY-NC-ND 4.0

pubs.acs.org/biochemistry
Article

Energetics of the H-Bond Network in *Exiguobacterium sibiricum* Rhodopsin

Tomoyasu Noji, Yoshihiro Chiba, Keisuke Saito, and Hiroshi Ishikita*

Cite This: *Biochemistry* 2024, 63, 1505−1512
Read Online

ACCESS | Metrics & More | Article Recommendations | Supporting Information

ABSTRACT: *Exiguobacterium sibiricum* rhodopsin (ESR) functions as a light-driven proton pump utilizing Lys96 for proton uptake and maintaining its activity over a wide pH range. Using a combination of methodologies including the linear Poisson−Boltzmann equation and a quantum mechanical/molecular mechanical approach with a polarizable continuum model, we explore the microscopic mechanisms underlying its pumping activity. Lys96, the primary proton uptake site, remains deprotonated owing to the loss of solvation in the ESR protein environment. Asp85, serving as a proton acceptor group for Lys96, does not form a low-barrier H-bond with His57. Instead, deprotonated Asp85 forms a salt-bridge with protonated His57, and the proton is predominantly located at the His57 moiety. Glu214, the only acidic residue at the end of the H-bond network exhibits a pK_a value of ∼6, slightly elevated due to solvation loss. It seems likely that the H-bond network [Asp85···His57···H_2O···Glu214] serves as a proton-conducting pathway toward the protein bulk surface.

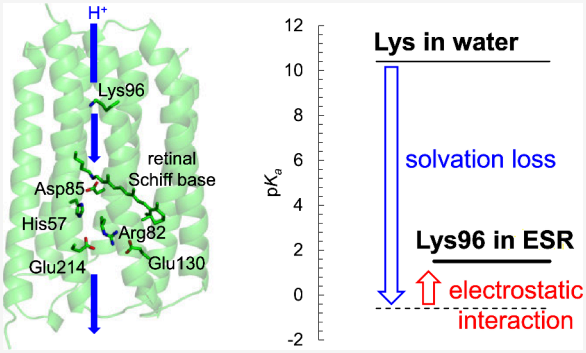

INTRODUCTION

The gene encoding *Exiguobacterium sibiricum* rhodopsin (ESR) was discovered in the genome of *Exiguobacterium sibiricum*, a Gram-positive eubacterium found in permafrost cores.[1] ESR functions a light-driven proton pump, using all-*trans* retinal Schiff base as its chromophore, and exhibits its proton pumping activity over a wide pH range of 4.5 to 8.5.[2,3] Despite structural similarities with bacteriorhodopsin (BR), a light-driven proton pump from the halophilic archaeon *Halobacterium salinarum*, ESR exhibits notable differences in its H-bond network. In BR, Asp85 is positioned near the retinal Schiff base, serving as a proton acceptor.[4,5] Similarly, the crystal structure of ESR shows that Asp85 is also located near the retinal Schiff base.[6] However, as observed in the entire proteorhodopsin family including proteorhodopsin and xanthorhodopsin, ESR incorporates His57 into the H-bond network with Asp85, forming an interaction with the retinal Schiff base (Figure 1). This feature contrasts with archaeal BR and *Acetabularia* rhodopsin, which lack this residue. While Arg82 orients toward Asp85 and forming a H-bond network with it via water molecules in the ground-state BR structure,[7] it orients away from the H-bond network of His57/Asp85 and instead forms a salt-bridge with Glu130 in the ESR structure.[6]

On the extracellular side of BR, Glu194 and Glu204 form a proton-sharing H-bond pair responsible for proton release toward the extracellular bulk surface.[8,9] However, these acidic residues are absent in the amino-acid sequence of ESR (e.g.,[10]). Structural comparison between the BR and ESR indicates that Glu204 in BR corresponds structurally to Glu214 in ESR, while Glu194 in BR is even structurally absent in ESR (Figure 1). Although Glu130 is the acidic residue nearest to Glu214 in ESR (6.0 Å), it does not form an H-bond with Glu214.[6] While a potential involvement of Glu214 in proton release has been pointed out by Siletsky et al.,[11] details remain unclear.

A significant difference is also observed on the intracellular side, where Asp96 functions as a proton uptake residue in BR,[12] yet is replaced by the basic residue Lys96 in ESR. Remarkably, mutational studies suggested that Lys96 serves as a proton uptake residue in ESR.[13] Despite mutations of Lys96 to carboxylic residues not affecting ESR functionality, their proton transfer mechanisms, including the rate-limiting step, remain distinct from those in BR.[14,15] These discrepancies in the H-bond network raise fundamental questions regarding how ESR compensates for the energetics of its proton-pumping activity, given the absence of essential components such as Asp96 for proton uptake and Glu194 and Glu204 for proton release in BR.

In this study, we investigate the protonation states and associated properties in ESR, using a combination of

Received: April 10, 2024
Revised: May 8, 2024
Accepted: May 8, 2024
Published: May 15, 2024

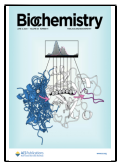

ACS Publications
© 2024 The Authors. Published by American Chemical Society

https://doi.org/10.1021/acs.biochem.4c00182
Biochemistry 2024, 63, 1505−1512

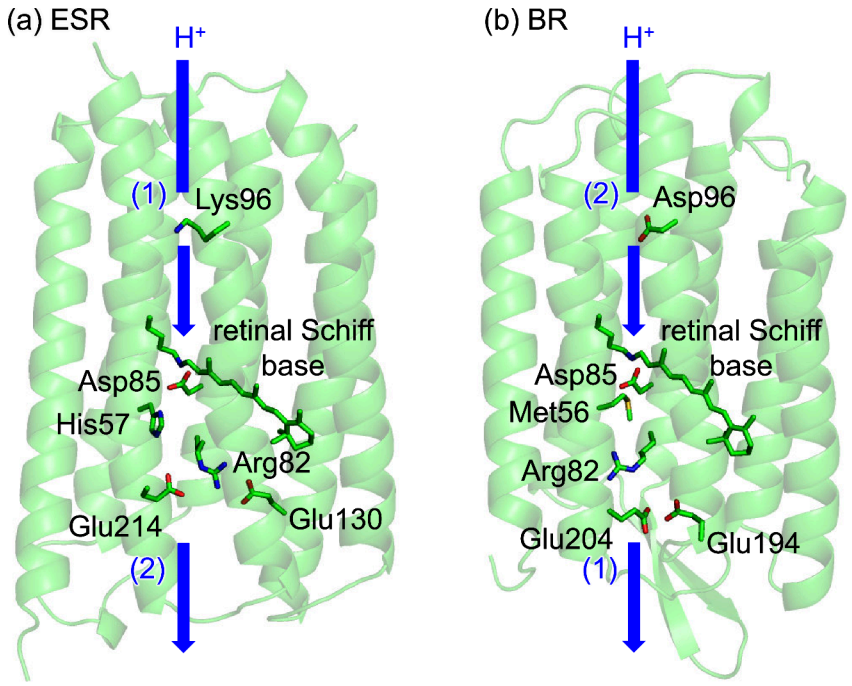

Figure 1. Proton transfer pathways of ESR and BR. (a) ESR. (b) BR. Blue arrows indicate directions of proton transfer. Numbers in brackets denote the sequence of events during proton transfer. In ESR, Lys96 is initially deprotonated and gains a proton before reprotonation of the retinal Schiff base. In contrast, in BR, reprotonation of the retinal Schiff base precedes reprotonation of Asp96 from the bulk. Notably, proton release toward the bulk occurs at the end of the photocycle in ESR, whereas it occurs at the beginning, during the M to N transition, in BR.

methodologies, including the linear Poisson−Boltzmann equation and a quantum mechanical/molecular mechanical approach (QM/MM) with a polarizable continuum model (PCM).

METHODS

Initial Geometry. For ESR, the atomic coordinates were obtained from the X-ray structure of ESR monomer unit "A" (PDB code, 4HYJ) corresponding to ESR conformations "2" in ref[6] unless otherwise specified. For BR, the atomic coordinates were obtained from the X-ray structure of the ground state (PDB code, 5J7A).[7] During the optimization process for hydrogen atom positions using CHARMM,[16] all heavy atom positions were kept fixed, and all titratable groups (e.g., acidic and basic groups) were ionized and the retinal Schiff base was protonated. Atomic partial charges for amino acids and the protonated retinal Schiff base were obtained from the CHARMM22 parameter set.[17]

Protonation Pattern and pK_a. The protonation pattern of the titratable residues was calculated by solving the linear Poisson−Boltzmann equation using the MEAD program.[18] All computations were performed at 300 K, pH 7.0, and an ionic strength of 100 mM. For pK_a calculations, crystal water molecules were removed, while implicit consideration of water molecules was implemented using a dielectric constant of 80. To determine the pK_a values of titratable sites in the protein, the calculated pK_a difference between the protein site and the reference system was added to the known reference pK_a value. The experimentally measured pK_a values used as references were 12.0 for Arg, 4.0 for Asp, 9.5 for Cys, 4.4 for Glu, 10.4 for Lys, 9.6 for Tyr,[19] and 7.0 and 6.6 for the Nε and Nδ sites of His, respectively.[20−22] Protonation patterns were sampled using a Monte Carlo method with Karlsberg.[23] The linear Poisson−Boltzmann equation was solved through a three-step grid-focusing procedure at resolutions of 2.5 Å, 1.0 Å, and 0.3 Å. Monte Carlo sampling provided the probabilities ([protonated] and [deprotonated]) for the two protonation states. The pK_a value was evaluated using the Henderson−Hasselbalch equation. A bias potential was applied to equalize both protonation states ([protonated] = [deprotonated]), yielding the pK_a value as the resulting bias potential. During titration of the focusing residue for pK_a, all other titratable sites were fully equilibrated to the protonation state of the focusing site.

QM/MM Calculations for Geometry Optimization. Geometry optimization was performed using a QM/MM approach. The restricted density functional theory (DFT) method was employed with the B3LYP functional and LACVP* basis sets using the QSite[24] program. To model the H57M mutant structure of ESR, the histidine side-chain was replaced with methionine, and the QM region was defined as side-chains of Met57, Asp85, and Thr89, and a water molecule at the Schiff base moiety (H_2O-402). To investigate the H-bond network of Lys96, the QM region was defined to include the side-chain of Lys96, the backbone groups of Ala47, Ala48, Lys225, and Val226, and water molecules at the Schiff base moiety (H_2O-502 and 503). For absorption-energy calculations, the QM region was defined as the retinal Schiff base (including the Lys225 side-chain), as previously used for 13 microbial rhodopsins.[25] All other protein components and water molecules involved in the H-bond network of the retinal Schiff base (H_2O-402, and H_2O-406) in the ESR crystal structure were included in the MM region. Atomic coordinates were fully relaxed in the QM region, and the protonation pattern of titratable residues was considered in the atomic partial charges of the corresponding MM region. In the MM region, the positions of H atoms were optimized using the

https://doi.org/10.1021/acs.biochem.4c00182
Biochemistry 2024, 63, 1505−1512

OPLS2005 force field,[26] while the positions of heavy atoms were kept fixed.

For the analysis of the potential-energy profile for the H-bond between His57 and Asp85, the QM region was defined as the retinal Schiff base (including the Lys225 side-chain), side-chains of His57, Arg82, Asp85, Trp86, Thr89, Asp221, and Glu214, and water molecules at the Schiff base moiety (H_2O-402, 403, 406, and 407). All other protein components and water molecules in the ESR crystal structure were included in the MM region. See the Supporting Information for the atomic coordinates of the QM/MM-optimized structures.

QM/MM Calculations for Absorption Energy. The absorption energy of microbial rhodopsins, including heliorhodopsin,[27] exhibits a strong correlation with the energy gap between the highest occupied molecular orbital (HOMO) and the lowest unoccupied molecular orbital (LUMO) ($E_{HOMO-LUMO}$), or the lowest excitation energy of the retinal Schiff base, which can be calculated using time-dependent (TD) DFT ($E_{TD\text{-}DFT}$).[25] This approach explicitly incorporates the electrostatic and steric effects induced by the protein environment in the presence of bulk water, employing a dielectric constant of 78 for the bulk region. To calculate the absorption energy and corresponding wavelength of ESR, $E_{HOMO-LUMO}$ and $E_{TD\text{-}DFT}$ were initially calculated using a QM/MM/PCM approach. Using eqs 1 and 2 derived for 13 microbial rhodopsins,[25] the resulting $E_{HOMO-LUMO}$ and $E_{TD\text{-}DFT}$ values were converted to the absorption energies (E_{abs} in eV) that could be compared with experimentally measured absorption energy (with a coefficient of determination R^2 = 0.995 and 0.920, respectively):

$$E_{abs} = 1.360\Delta E_{HOMO-LUMO} - 1.018 \quad (1)$$

$$E_{abs} = 1.754E_{TD-DFT} - 2.073 \quad (2)$$

The corresponding absorption wavelength was then converted from the resulting E_{abs} value.

The PCM method used polarization points with a radius of 2.8 Å from the center of each atom to describe potential water molecules in the cavity. A radius of 2.8−3.0 Å from each atom center and a dielectric constant value of ∼80 are considered optimal to accurately reproduce the excitation energetics, as assessed for the polarizable QM/MM/PCM approach.[28] The TD-DFT method with the B3LYP functional and 6-31G* basis sets was employed using the GAMESS program.[29]

QM/MM Calculations for Potential-Energy Profile. To analyze the potential energy profiles of the H-bond between His57 and Asp85, the initial geometry was derived from the QM/MM-optimized geometry. A focusing H atom was incrementally moved along the N···H^+···O bond by 0.05 Å. After each displacement, the geometry was optimized while keeping the N···H and H···O distances fixed, and the resulting energy was calculated. This iterative procedure continued until the H atom reached the proton donor N or acceptor O moieties.

RESULTS AND DISCUSSION

His57 and Asp85. The protonation pattern, calculated by solving the linear Poisson−Boltzmann equation, indicate that His57 is doubly protonated (with protons at both Nδ and Nε sites), while Asp85 is fully deprotonated at pH 7.0, forming a salt-bridge (Table 1). Calculated pK_a values are 9.6 for His57 and 0.1 for Asp85 (Table 1). The experimentally measured values are pK_a(His57) = 9 and pK_a(Asp85) = 2.3 for ESR solubilized in detergent (dodecyl maltoside),[3] and pK_a(His57) = 6.5 for ESR in lipid.[3,10,13] The calculated pK_a(His57) value is closer to the value measured in detergent than that in lipid, which suggests that that the protein environment for His57 in the ESR crystal structure may resemble the protein environment in detergent. Spectroscopic studies indicated a significant increase in the pK_a value of Asp85 to 6.3 upon the H57M mutation.[3] While the calculated pK_a(Asp85) value of 4.6 in the H57M structure is slightly lower than the experimentally measured value of 6.3 in H57M mutant ESR (Table 1), the significant increase observed upon the replacement of His57 with methionine in the present calculation is in line with the experimental result, indicating that His57 decreases pK_a(Asp) in wild type ESR.

Table 1. Calculated pK_a Values and Protonation Probabilities for Titratable Residues in Wild Type and H57M mutant ESRs[a]

	wild type		H57M	
	pK_a	H^+ probability	pK_a	H^+ probability
His57	9.6	1.00	–	–
Asp85	0.1	0.00	4.6	0.00
Lys96	1.5	0.00	1.7	0.00
Glu214	5.6	0.04	8.7	0.98

[a]–: not applicable.

Although the possible existence of a low-barrier H-bond between His57 and Asp85 was debated based on the H-bond distance of 2.6 to 2.7 Å identified in the ESR crystal structures,[6] the shape of the potential energy curve for this H-bond appears asymmetric (Figure 2), which is in contrast to the symmetric shape observed in low-barrier H-bonds.[30−33] Furthermore, the significant difference in pK_a values between these two residues is in contrast to nearly similar pK_a values for the H-bond donor and acceptor moieties required for a low-barrier H-bond. As the calculated pK_a difference (Table 1) is substantially consistent with the experimentally measured pK_a difference,[3] this conclusion is likely to remain unchanged even if higher resolution structures are obtained.

Indeed, in cases where histidine participates in a low-barrier H-bond, the H-bond distance is notably shorter, typically <2.5 Å (e.g., the D1-Tyr161 and D1-His190 pair[34] and the D1-His215 and quinone pair[35] in photosystem II). These observations indicate that the proton is predominantly stabilized and localized at the His57 moiety rather than being equally shared between the two residues. Therefore, the H-bond between His57 and Asp85 can unambiguously be explained as a standard H-bond (or a salt-bridge).

Lys96. In the ground-state ESR structure, Lys96 is fully deprotonated, exhibiting a calculated pK_a(Lys96) of 1.5 (Table 1), consistent with the proposed deprotonation of Lys96 based on its location in the hydrophobic cavity of the crystal structure.[6] To understand the significant decrease in pK_a(Lys96) from its typical value of 10.4 in water[19] to 1.5 in the protein environment of ESR, factors influencing pK_a(Lys96) in the ESR structure are investigated.

The loss of solvation (i.e., loss of bulk water) for titratable residues in protein environments generally destabilizes their charged states, favoring charge-neutral states, such as deprotonated basic residues and protonated acidic residues. In the ESR protein environment, the loss of solvation for Lys96 contributes most significantly to the decrease in pK_a(Lys96) by more than 11 units (Figure 3). Although electrostatic

https://doi.org/10.1021/acs.biochem.4c00182
Biochemistry 2024, 63, 1505−1512

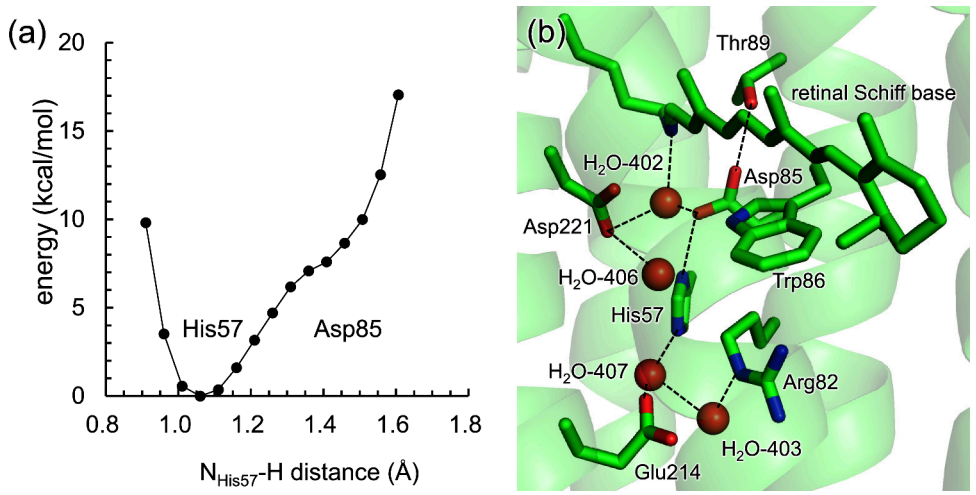

Figure 2. H-bond network at the retinal Schiff base moiety. (a) Potential-energy profile for the H-bond between His57 and Asp85. (b) Overview of the H-bond network in the ESR crystal structure. The QM region used for analysis is explicitly shown. Dotted lines indicate representative H-bonds.

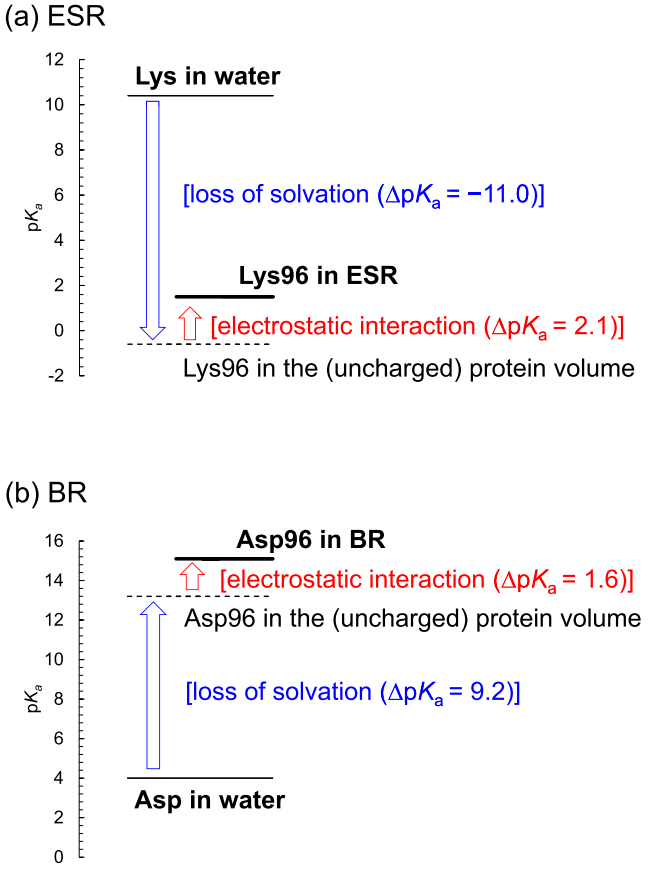

Figure 3. Factors influencing the shift in pK_a for the proton uptake site. (a) pK_a(Lys96) in ESR. (b) pK_a(Asp96) in BR.

interactions with residues like Ala232 (−1.4, mainly from the backbone group), Ala47 (−0.8, mainly from the backbone group), and the retinal Schiff base (−0.8) also contribute to the decrease in pK_a(Lys96), these effects are mostly counteracted by electrostatic interactions with other residues, such as Thr43 (1.9) and Asp85 (0.8), Asp221 (0.8), and Phe228 (0.8, mainly from the backbone group) (Table 2). Consequently, the overall electrostatic interaction with the ESR protein environment results in a modest increase in pK_a(Lys96) by 2

Table 2. Residues Influencing the Shift in pK_a(Lys96) More than 0.5 pK_a Units

decreasing pK_a(Lys96)		increasing pK_a(Lys96)	
Ala232	−1.4	Thr43	1.9
Ala47	−0.8	Asp85	0.8
retinal + Lys225	−0.8	Asp221	0.8
Leu99	−0.5	Phe228	0.8
Val46	−0.5	Ser42	0.7
		Leu92	0.7
		Val226	0.6
		Leu93	0.6
		Ala44	0.5
		Leu230	0.5
		Gly229	0.5

units (Figure 3). Thus, the deprotonation of Lys96 is primarily attributed to its reduced solvation in the protein environment of ESR.

Despite the significant contribution of solvation loss (i.e., loss of bulk water) to the decrease in pK_a(Lys96), the ESR crystal structure reveals the presence of a water molecule (H$_2$O-503) adjacent to Lys96 (N$_{Lys96}$...O$_{water}$ = 2.92 Å).[6] Unlike bulk water molecules, which can adopt various orientations, H$_2$O-503 functions as a fixed dipole in the small cavity, evident from its relatively low *B*-factor of 29. Indeed, the present QM/MM calculation further demonstrates that H$_2$O-503 donates an H-bond to deprotonated Lys96 (Figure 4), contributing a decrease in pK_a(Lys96), in contrast to the role of bulk water molecules, which elevate pK_a(Lys96) to10.4.[19]

The calculated pK_a(Lys96) value of 1.5 in the ground state is significantly lower than the experimentally measured pK_a(Lys96) value of 8.5 in the M state.[13] Although the M-state structure has not been reported, the difference in pK_a(Lys96) implies that Lys96 becomes more exposed to the bulk solvent in the M state than in the ground state, likely due to light-induced structural changes.

The solvation-loss environment for Lys96 in the ground-state ESR structure is distinct, even when compared with other protein environments housing deprotonated lysine, such as the catalytic deprotonated lysine (Lys115) in acetoacetate

https://doi.org/10.1021/acs.biochem.4c00182
Biochemistry 2024, 63, 1505−1512

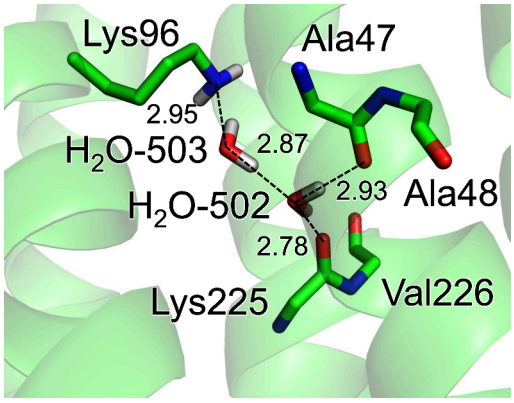

Figure 4. QM/MM-optimized geometry for the H-bond network of deprotonated Lys96. Dotted lines with numerical values indicate H-bonds with distances in Å.

decarboxylase (AADase).[36,37] Both experimentally measured[36] and calculated[38] pK_a(Lys115) values are 6, as indicated by the packed protein environment for Lys115 in the AADase crystal structure.[39] The contribution of solvation loss to pK_a(Lys115) in AADase is 8 units, whereas for pK_a(Lys96) in ESR, it amounts to 11 units. The higher solvation accessibility for Lys115 in the ground-state AADase structure likely arises from its role as the catalytic site in the water-soluble enzyme, facilitating substrate binding.

The replacement of Lys96 in ESR with Asp96 in BR, both serving as proton uptake residues, is noteworthy. Comparisons of factors influencing their pK_a values may provide further insight into their characteristics. In contrast to low pK_a(Lys96) in the ESR structure, the calculated pK_a(Asp96) value in the ground-state BR structure[7] is significantly high, 15.1,[40] as suggested in spectroscopic studies (>12[12]). In BR, the high pK_a(Asp96) value is primarily influenced by the loss of solvation in the protein environment, contributing to an increase in pK_a(Asp96) by 9 units (Figure 3). Thus, the upshift in pK_a(Asp96) in BR and the downshift in pK_a(Lys96) in ESR share a common origin: their hydrophobic protein environments stabilize their uncharged protonation states, leading to deprotonated Lys96 in ESR and protonated Asp96 in BR.

The absorption wavelength calculated using the ESR structure is 528 nm (excitation energy) and 531 nm (HOMO−LUMO energy gap) with deprotonated Lys96, and 534 nm (excitation energy) and 541 nm (HOMO−LUMO energy gap) with protonated Lys96 (Figure 5), which closely approximate the experimentally measured absorption wavelength of 531 nm.[3] These results indicates that the protonation state of Lys96 has minimal impact on the absorption wavelength of ESR due to the long distance (>12 Å) between Lys96 and the retinal Schiff base.

Previous theoretical studies suggest a strong correlation between absorption energies and HOMO−LUMO energy gaps among microbial rhodopsins.[25,40] The present study confirms that this correlation also holds true for ESR (Figure 5), which suggests that the absorption wavelength of ESR is primarily determined by its HOMO−LUMO energy gap.

Glu214. In BR, Glu194 and Glu204 form an H-bond (Figure 6b). The reported pK_a values or protonation states in BR indicates that one of the two glutamates is protonated, with the proton shared between them.[40−43] Notably, a similar pair of glutamates, D1-Glu65 and D2-Glu312, share a proton and serves as a terminal component in the proton-conducting

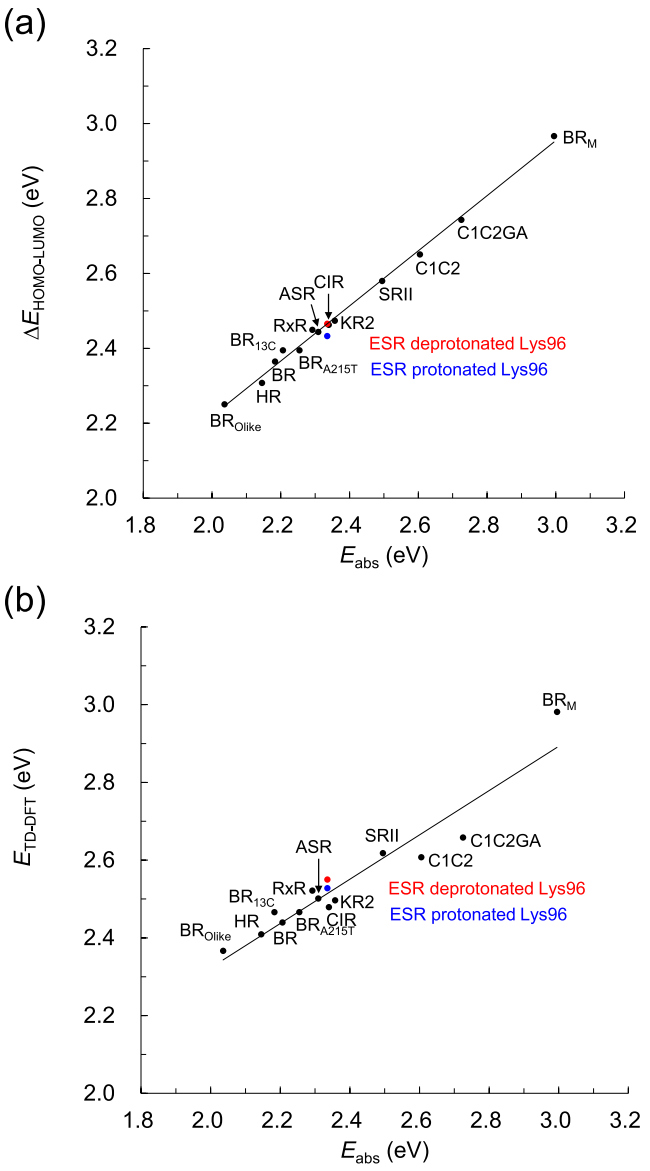

Figure 5. Absorption energies in microbial rhodopsins. (a) Correlation between calculated HOMO−LUMO energy difference ($\Delta E_{HOMO-LUMO}$) and experimentally measured absorption energy (E_{abs} = 1.360 $\Delta E_{HOMO-LUMO}$ − 1.018: coefficient of determination R^2 = 0.995[25]). (b) Correlation between the lowest excitation energy values ($E_{TD\text{-}DFT}$) calculated using the TD-DFT method and experimentally measured absorption energy (E_{abs} = 1.754 $E_{TD\text{-}DFT}$ − 2.073: R^2 = 0.920[25]). Red and blue closed circles indicate ESR with deprotonated and protonated Lys96, respectively. Black closed circles represent other microbial rhodopsins investigated previously;[25] ASR: *Anabaena* sensory rhodopsin; BR: *Halobacterium salinaru* bacteriorhodopsin with all-*trans* retinal Schiff base; $BR_{13\text{-}cis}$: BR with 13-*cis* retinal Schiff base; BR_{A215T}: A215T mutant BR; BR_M: M-state intermediate of BR; BR_{D85S}: D85S mutant BR; C1C2: channelrhodopsin-2 from *Chlamydomonas reinhardtii*; ClR: eubacterial chloride-pumping rhodopsin; HR: archeal chloride-pumping halorhodopsin; KR2: sodium pump rhodopsin from *Krokinobacter eikastus*; RxR: *Rubrobacter xylanophilus* rhodopsin; SRII: sensory rhodopsin II.

pathway originating from the substrate water molecules in photosystem II (PSII)[44,45] (Figure 6c). Drawing on this analogy, protonation of acidic residues at the terminus region of the proton-conducting pathway appears to be a common feature. While the corresponding pair is not conserved in ESR,

https://doi.org/10.1021/acs.biochem.4c00182
Biochemistry 2024, 63, 1505−1512

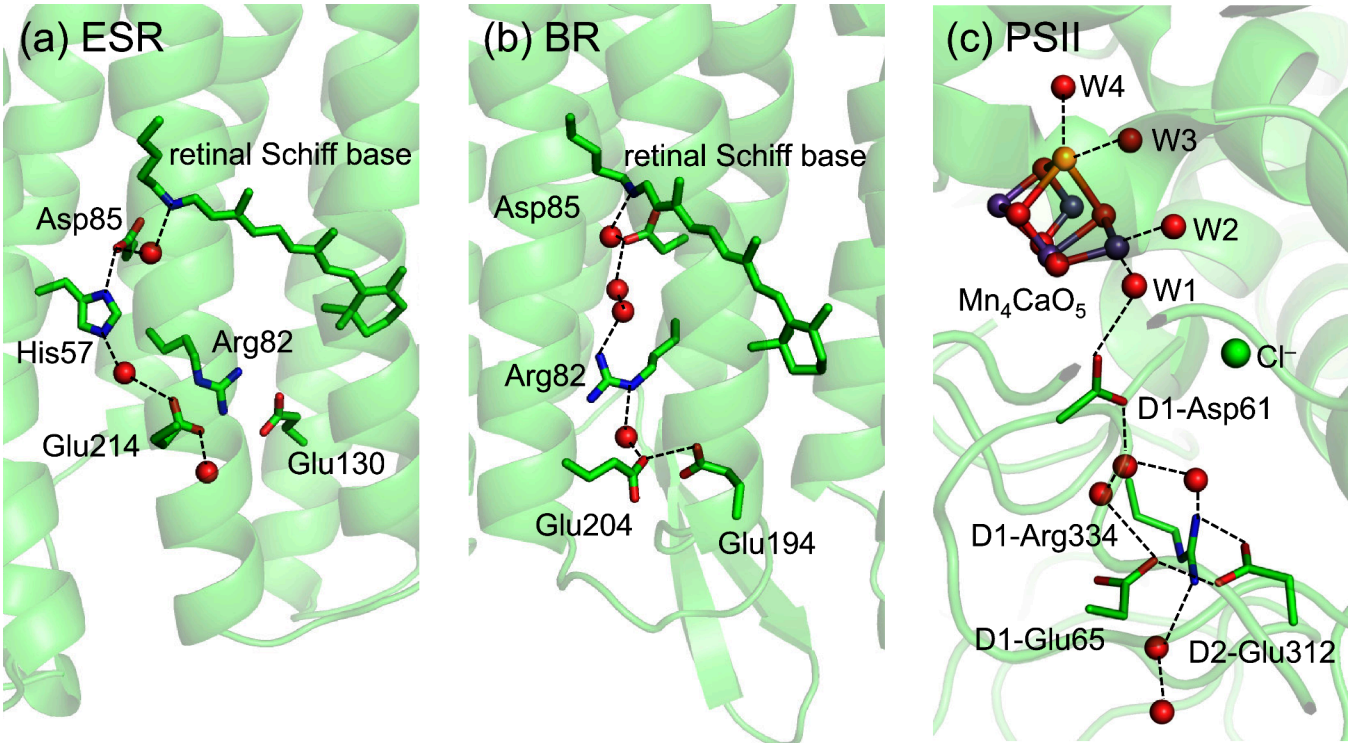

Figure 6. Comparison of H-bond networks for proton-exit pathways. (a) ESR (PDB code, 4HYJ).[6] (b) BR (PDB code, 5J7A).[7] (c) Water-splitting enzyme, photosystem II (PSII) (PDB code, 3WU2).[46] In PSII, the ligand water molecule W1 at the catalytic site Mn_4CaO_5 forms a low-barrier H-bond with D1-Asp61, releasing the proton.[47,48] Dotted lines indicate representative electrostatic interactions, including H-bonds.

Glu214 occupies a position at the terminal region of the H-bond network.

The present study indicates that Glu214 is partially protonated at pH 7.0 with pK_a(Glu214) of 5.6 (Table 1). Although the exact pK_a value for Glu214 has not been reported, among all acidic residues in ESR, the calculated pK_a(Glu214) value is the closest to the pK_a value of 6 for the unidentified residue reported in spectroscopic studies by Balashov et al.[3] During pH titration, an increase in solvent pH resulted in a blue shift of 3 nm associated with the pK_a value of 6 owing to deprotonation of the unidentified residue.[3] Intriguingly, the calculated absorption wavelength is 3−4 nm shorter in the presence of fully deprotonated Glu214 than in the presence of fully protonated Glu214 (Table 3). The substantially similar shift in the absorption wavelength upon deprotonation of Glu214 suggests that Glu214 is a likely candidate for the residue with the reported pK_a value of 6. While it was discussed in ref[3] that the pK_a value of 6 could originate from partial protonation of Asp85, it seems possible that this partial protonation may arise from interactions with other ionizable groups, primarily His57, and possibly Glu214.

Table 3. Calculated Absorption Wavelengths in Different Protonation States of Glu214 (nm)

Glu214	wavelength		
H^+state	H^+probability	excitation energy	HOMO−LUMO
protonated	1.00	530	534
pH 7	0.04	528	531
deprotonated	0.00	528	531

In contrast to Glu194 and Glu204 in BR, Glu214 is not located on the protein bulk surface but is instead buried in the protein interior, forming part of a cluster of ionizable and polar side chains, including Arg82, Glu130, Arg213, Glu214, and Gln210.[6] Therefore, while the observed slight increase in pK_a(Glu214) is primarily attributed to the loss of solvation in the protein environment (Figure 7), its impact on pK_a(Glu214) (= 6.2) is considerably smaller than on pK_a(Lys96) (=11.0, Figure 3). Given that an elevated pK_a in the terminal region of the proton-conducting pathway is beneficial for generating the driving force for proton transfer toward the protein bulk surface,[44,49,50] the slightly high pK_a(Glu214) in ESR may indicate its potential role in serving as a similar function to Glu194 and Glu204 in BR.

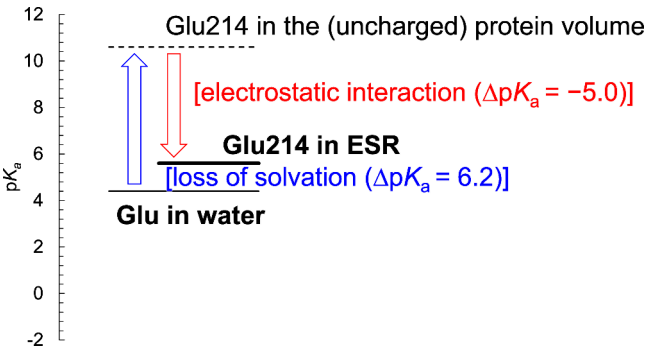

Figure 7. Factors influencing the shift in pK_a(Glu214) in ESR.

CONCLUSIONS

The calculated pK_a values of 9.6 for His57 and 0.1 for Asp85 (Table 1) are consistent with experimentally measured values.[3] Analysis of the potential-energy curve for the H-bond between

https://doi.org/10.1021/acs.biochem.4c00182
Biochemistry 2024, 63, 1505−1512

His57 and Asp85 reveals an asymmetric shape, indicating the formation of a standard H-bond rather than a low-barrier H-bond (Figure 2). The significant difference in pK_a values (Table 1), suggesting the predominant localization of the proton at the His57 moiety, further supports this observation. The calculated pK_a value for Lys96 is 1.5, and Lys96 is fully deprotonated due to the loss of solvation in the protein environment (Table 1). The absorption wavelength calculated using the ESR crystal structure closely matches the experimentally measured absorption wavelength,[51] regardless of the protonation state of Lys96. While spectroscopic studies reported the presence of a residue with a pK_a value of 6,[3] the calculated pK_a value of Glu214 at the terminus of the H-bond network is the closest among all acidic residues in the ESR crystal structure (Table 1). While the slight increase in pK_a(Glu214) is attributed not to electrostatic interaction with adjacent acidic residues (e.g., Glu194/Glu204 in BR) but rather to the loss of solvation in the ESR protein environment (Figure 7), its slightly elevated pK_a suggests its potential role in the terminus region of the proton-conducting wire. These characteristics of ESR may provide insights into its less pH-sensitive proton-pumping activity compared to BR, which operates effectively in a broad pH range.[2,3]

■ ASSOCIATED CONTENT

Supporting Information

The Supporting Information is available free of charge at https://pubs.acs.org/doi/10.1021/acs.biochem.4c00182.

QM/MM-optimized structure of ESR (PDF)

■ AUTHOR INFORMATION

Corresponding Author

Hiroshi Ishikita − *Department of Applied Chemistry, The University of Tokyo, Tokyo 113-8654, Japan; Research Center for Advanced Science and Technology, The University of Tokyo, Tokyo 153-8904, Japan;* orcid.org/0000-0002-5849-8150; Phone: +81-3-5452-5056; Email: hiro@appchem.t.u-tokyo.ac.jp; Fax: +81-3-5452-5083

Authors

Tomoyasu Noji − *Department of Applied Chemistry, The University of Tokyo, Tokyo 113-8654, Japan; Research Center for Advanced Science and Technology, The University of Tokyo, Tokyo 153-8904, Japan;* orcid.org/0000-0001-9468-2038

Yoshihiro Chiba − *Department of Applied Chemistry, The University of Tokyo, Tokyo 113-8654, Japan*

Keisuke Saito − *Department of Applied Chemistry, The University of Tokyo, Tokyo 113-8654, Japan; Research Center for Advanced Science and Technology, The University of Tokyo, Tokyo 153-8904, Japan;* orcid.org/0000-0002-2293-9743

Complete contact information is available at: https://pubs.acs.org/10.1021/acs.biochem.4c00182

Notes

The authors declare no competing financial interest.

■ ACKNOWLEDGMENTS

This research was supported by JSPS KAKENHI (JP23H04963 and 24K01986 to K.S.; JP23H02444 to H.I.) and Interdisciplinary Computational Science Program in CCS, University of Tsukuba.

■ REFERENCES

(1) Rodrigues, D. F.; Ivanova, N.; He, Z.; Huebner, M.; Zhou, J.; Tiedje, J. M. Architecture of thermal adaptation in an *Exiguobacterium sibiricum* strain isolated from 3 million year old permafrost: A genome and transcriptome approach. *BMC Genomics* **2008**, *9*, 547.

(2) Petrovskaya, L. E.; Lukashev, E. P.; Chupin, V. V.; Sychev, S. V.; Lyukmanova, E. N.; Kryukova, E. A.; Ziganshin, R. H.; Spirina, E. V.; Rivkina, E. M.; Khatypov, R. A.; Erokhina, L. G.; Gilichinsky, D. A.; Shuvalov, V. A.; Kirpichnikov, M. P. Predicted bacteriorhodopsin from *Exiguobacterium sibiricum* is a functional proton pump. *FEBS Lett.* **2010**, *584*, 4193−4196.

(3) Balashov, S. P.; Petrovskaya, L. E.; Lukashev, E. P.; Imasheva, E. S.; Dioumaev, A. K.; Wang, J. M.; Sychev, S. V.; Dolgikh, D. A.; Rubin, A. B.; Kirpichnikov, M. P.; Lanyi, J. K. Aspartate−histidine interaction in the retinal Schiff base counterion of the light-driven proton pump of *Exiguobacterium sibiricum*. *Biochemistry* **2012**, *51*, 5748−5762.

(4) Maeda, A.; Sasaki, J.; Yamazaki, Y.; Needleman, R.; Lanyi, J. K. Interaction of aspartate-85 with a water molecule and the protonated Schiff base in the L intermediate of bacteriorhodopsin: a Fourier-transform infrared spectroscopic study. *Biochemistry* **1994**, *33*, 1713−1717.

(5) Kandori, H.; Yamazaki, Y.; Sasaki, J.; Needleman, R.; Lanyi, J. K.; Maeda, A. Water-mediated proton transfer in proteins: an FTIR study of bacteriorhodopsin. *J. Am. Chem. Soc.* **1995**, *117*, 2118−2119.

(6) Gushchin, I.; Chervakov, P.; Kuzmichev, P.; Popov, A. N.; Round, E.; Borshchevskiy, V.; Ishchenko, A.; Petrovskaya, L.; Chupin, V.; Dolgikh, D. A.; Arseniev, A. S.; Kirpichnikov, M.; Gordeliy, V. Structural insights into the proton pumping by unusual proteorhodopsin from nonmarine bacteria. *Proc. Natl. Acad. Sci. U. S. A.* **2013**, *110*, 12631−12636.

(7) Nogly, P.; Panneels, V.; Nelson, G.; Gati, C.; Kimura, T.; Milne, C.; Milathianaki, D.; Kubo, M.; Wu, W.; Conrad, C.; Coe, J.; Bean, R.; Zhao, Y.; Båth, P.; Dods, R.; Harimoorthy, R.; Beyerlein, K. R.; Rheinberger, J.; James, D.; DePonte, D.; Li, C.; Sala, L.; Williams, G. J.; Hunter, M. S.; Koglin, J. E.; Berntsen, P.; Nango, E.; Iwata, S.; Chapman, H. N.; Fromme, P.; Frank, M.; Abela, R.; Boutet, S.; Barty, A.; White, T. A.; Weierstall, U.; Spence, J.; Neutze, R.; Schertler, G.; Standfuss, J. Lipidic cubic phase injector is a viable crystal delivery system for time-resolved serial crystallography. *Nat. Commun.* **2016**, *7*, 12314.

(8) Balashov, S. P. Protonation reactions and their coupling in bacteriorhodopsin. *Biochim. Biophys. Acta* **2000**, *1460*, 75−94.

(9) Kandori, H. Role of internal water molecules in bacteriorhodopsin. *Biochim. Biophys. Acta* **2000**, *1460*, 177−191.

(10) Dioumaev, A. K.; Petrovskaya, L. E.; Wang, J. M.; Balashov, S. P.; Dolgikh, D. A.; Kirpichnikov, M. P.; Lanyi, J. K. Photocycle of *Exiguobacterium sibiricum* rhodopsin characterized by low-temperature trapping in the IR and time-resolved studies in the visible. *J. Phys. Chem. B* **2013**, *117*, 7235−7253.

(11) Siletsky, S. A.; Lukashev, E. P.; Mamedov, M. D.; Borisov, V. B.; Balashov, S. P.; Dolgikh, D. A.; Rubin, A. B.; Kirpichnikov, M. P.; Petrovskaya, L. E. His57 controls the efficiency of ESR, a light-driven proton pump from *Exiguobacterium sibiricum* at low and high pH. *Biochim. Biophys. Acta* **2021**, *1862*, 148328.

(12) Zscherp, C.; Schlesinger, R.; Tittor, J.; Oesterhelt, D.; Heberle, J. *In situ* determination of transient pK_a changes of internal amino acids of bacteriorhodopsin by using time-resolved attenuated total reflection Fourier-transform infrared spectroscopy. *Proc. Natl. Acad. Sci. U. S. A.* **1999**, *96*, 5498−5503.

(13) Balashov, S. P.; Petrovskaya, L. E.; Imasheva, E. S.; Lukashev, E. P.; Dioumaev, A. K.; Wang, J. M.; Sychev, S. V.; Dolgikh, D. A.; Rubin, A. B.; Kirpichnikov, M. P.; Lanyi, J. K. Breaking the carboxyl rule: lysine 96 facilitates reprotonation of the Schiff base in the photocycle of a retinal protein from *Exiguobacterium sibiricum*. *J. Biol. Chem.* **2013**, *288*, 21254−21265.

(14) Sasaki, S.; Tamogami, J.; Nishiya, K.; Demura, M.; Kikukawa, T. Replaceability of Schiff base proton donors in light-driven proton pump rhodopsins. *J. Biol. Chem.* **2021**, *297*, 101013.
(15) Petrovskaya, L. E.; Lukashev, E. P.; Siletsky, S. A.; Imasheva, E. S.; Wang, J. M.; Mamedov, M. D.; Kryukova, E. A.; Dolgikh, D. A.; Rubin, A. B.; Kirpichnikov, M. P.; Balashov, S. P.; Lanyi, J. K. Proton transfer reactions in donor site mutants of ESR, a retinal protein from *Exiguobacterium sibiricum*. *J. Photochem. Photobiol. B* **2022**, *234*, 112529.
(16) Brooks, B. R.; Bruccoleri, R. E.; Olafson, B. D.; States, D. J.; Swaminathan, S.; Karplus, M. CHARMM: a program for macromolecular energy, minimization, and dynamics calculations. *J. Comput. Chem.* **1983**, *4*, 187−217.
(17) MacKerell, A. D., Jr.; Bashford, D.; Bellott, R. L.; Dunbrack, R. L., Jr.; Evanseck, J. D.; Field, M. J.; Fischer, S.; Gao, J.; Guo, H.; Ha, S.; Joseph-McCarthy, D.; Kuchnir, L.; Kuczera, K.; Lau, F. T. K.; Mattos, C.; Michnick, S.; Ngo, T.; Nguyen, D. T.; Prodhom, B.; Reiher, W. E., III; Roux, B.; Schlenkrich, M.; Smith, J. C.; Stote, R.; Straub, J.; Watanabe, M.; Wiorkiewicz-Kuczera, J.; Yin, D.; Karplus, M. All-atom empirical potential for molecular modeling and dynamics studies of proteins. *J. Phys. Chem. B* **1998**, *102*, 3586−3616.
(18) Bashford, D.; Karplus, M. pK_a's of ionizable groups in proteins: atomic detail from a continuum electrostatic model. *Biochemistry* **1990**, *29*, 10219−10225.
(19) Nozaki, Y.; Tanford, C. Acid-base titrations in concentrated guanidine hydrochloride. Dissociation constants of the guanidinium ion and of some amino acids. *J. Am. Chem. Soc.* **1967**, *89*, 736−742.
(20) Tanokura, M. ^{1}H nuclear magnetic resonance titration curves and microenvironments of aromatic residues in bovine pancreatic ribonuclease A. *J. Biochem.* **1983**, *94*, 51−62.
(21) Tanokura, M. ^{1}H-NMR study on the tautomerism of the imidazole ring of histidine residues: I. Microscopic p*K* values and molar ratios of tautomers in histidine-containing peptides. *Biochim. Biophys. Acta* **1983**, *742*, 576−585.
(22) Tanokura, M. ^{1}H-NMR study on the tautomerism of the imidazole ring of histidine residues: II. Microenvironments of histidine-12 and histidine-119 of bovine pancreatic ribonuclease a. *Biochim. Biophys. Acta* **1983**, *742*, 586−596.
(23) Rabenstein, B.; Knapp, E.-W. Calculated pH-dependent population and protonation of carbon-monoxy-myoglobin conformers. *Biophys. J.* **2001**, *80*, 1141−1150.
(24) *QSite*, version 5.8; Schrödinger, LLC: New York, NY, 2012.
(25) Tsujimura, M.; Ishikita, H. Insights into the protein functions and absorption wavelengths of microbial rhodopsins. *J. Phys. Chem. B* **2020**, *124*, 11819−11826.
(26) Jorgensen, W. L.; Maxwell, D. S.; Tirado-Rives, J. Development and testing of the OPLS all-atom force field on conformational energetics and properties of organic liquids. *J. Am. Chem. Soc.* **1996**, *118*, 11225−11236.
(27) Tsujimura, M.; Chiba, Y.; Saito, K.; Ishikita, H. Proton transfer and conformational changes along the hydrogen bond network in heliorhodopsin. *Commun. Biol.* **2022**, *5*, 1336.
(28) Tamura, H.; Saito, K.; Ishikita, H. Acquirement of water-splitting ability and alteration of the charge-separation mechanism in photosynthetic reaction centers. *Proc. Natl. Acad. Sci. U. S. A.* **2020**, *117*, 16373−16382.
(29) Schmidt, M. W.; Baldridge, K. K.; Boatz, J. A.; Elbert, S. T.; Gordon, M. S.; Jensen, J. H.; Koseki, S.; Matsunaga, N.; Nguyen, K. A.; Su, S. J.; Windus, T. L.; Dupuis, M.; Montgomery, J. A. General atomic and molecular electronic-structure system. *J. Comput. Chem.* **1993**, *14*, 1347−1363.
(30) Warshel, A.; Papazyan, A.; Kollman, P. A. On low-barrier hydrogen bonds and enzyme catalysis. *Science* **1995**, *269*, 102−106.
(31) Perrin, C. L.; Nielson, J. B. "Strong" hydrogen bonds in chemistry and biology. *Annu. Rev. Phys. Chem.* **1997**, *48*, 511−544.
(32) Schutz, C. N.; Warshel, A. The low barrier hydrogen bond (LBHB) proposal revisited: the case of the Asp···His pair in serine proteases. *Proteins* **2004**, *55*, 711−723.
(33) Ishikita, H.; Saito, K. Proton transfer reactions and hydrogen-bond networks in protein environments. *J. R. Soc. Interface* **2014**, *11*, 20130518.
(34) Saito, K.; Shen, J.-R.; Ishida, T.; Ishikita, H. Short hydrogen-bond between redox-active tyrosine Y_Z and D1-His190 in the photosystem II crystal structure. *Biochemistry* **2011**, *50*, 9836−9844.
(35) Saito, K.; Rutherford, A. W.; Ishikita, H. Mechanism of proton-coupled quinone reduction in Photosystem II. *Proc. Natl. Acad. Sci. U. S. A.* **2013**, *110*, 954−959.
(36) Kokesh, F. C.; Westheimer, F. H. A reporter group at the active site of acetoacetate decarboxylase. II. Ionization constant of the amino group. *J. Am. Chem. Soc.* **1971**, *93*, 7270−7274.
(37) Gerlt, J. A. Acetoacetate decarboxylase: hydrophobics, not electrostatics. *Nat. Chem. Biol.* **2009**, *5*, 454−455.
(38) Ishikita, H. Origin of the pK_a shift of the catalytic lysine in acetoacetate decarboxylase. *FEBS Lett.* **2010**, *584*, 3464−3468.
(39) Ho, M. C.; Menetret, J. F.; Tsuruta, H.; Allen, K. N. The origin of the electrostatic perturbation in acetoacetate decarboxylase. *Nature* **2009**, *459*, 393−397.
(40) Noji, T.; Ishikita, H. Mechanism of absorption wavelength shift of bacteriorhodopsin during photocycle. *J. Phys. Chem. B* **2022**, *126*, 9945−9955.
(41) Balashov, S. P.; Imasheva, E. S.; Govindjee, R.; Ebrey, T. G. Titration of aspartate-85 in bacteriorhodopsin: what it says about chromophore isomerization and proton release. *Biophys. J.* **1996**, *70*, 473−481.
(42) Richter, H. T.; Brown, L. S.; Needleman, R.; Lanyi, J. K. A linkage of the pK_a's of asp-85 and glu-204 forms part of the reprotonation switch of bacteriorhodopsin. *Biochemistry* **1996**, *35*, 4054−4062.
(43) Dioumaev, A. K.; Richter, H. T.; Brown, L. S.; Tanio, M.; Tuzi, S.; Saito, H.; Kimura, Y.; Needleman, R.; Lanyi, J. K. Existence of a proton transfer chain in bacteriorhodopsin: participation of Glu-194 in the release of protons to the extracellular surface. *Biochemistry* **1998**, *37*, 2496−2506.
(44) Ishikita, H.; Saenger, W.; Loll, B.; Biesiadka, J.; Knapp, E.-W. Energetics of a possible proton exit pathway for water oxidation in photosystem II. *Biochemistry* **2006**, *45*, 2063−2071.
(45) Kuroda, H.; Kawashima, K.; Ueda, K.; Ikeda, T.; Saito, K.; Ninomiya, R.; Hida, C.; Takahashi, Y.; Ishikita, H. Proton transfer pathway from the oxygen-evolving complex in photosystem II substantiated by extensive mutagenesis. *Biochim. Biophys. Acta* **2021**, *1862*, 148329.
(46) Umena, Y.; Kawakami, K.; Shen, J.-R.; Kamiya, N. Crystal structure of oxygen-evolving photosystem II at a resolution of 1.9 Å. *Nature* **2011**, *473*, 55−60.
(47) Kawashima, K.; Takaoka, T.; Kimura, H.; Saito, K.; Ishikita, H. O_2 evolution and recovery of the water-oxidizing enzyme. *Nat. Commun.* **2018**, *9*, 1247.
(48) Saito, K.; Nishio, S.; Ishikita, H. Interplay of two low-barrier hydrogen bonds in long-distance proton-coupled electron transfer for water oxidation. *PNAS Nexus* **2023**, *2*, No. pgad423.
(49) Saito, K.; Rutherford, A. W.; Ishikita, H. Energetics of proton release on the first oxidation step in the water-oxidizing enzyme. *Nat. Commun.* **2015**, *6*, 8488.
(50) Takaoka, T.; Sakashita, N.; Saito, K.; Ishikita, H. pK_a of a proton-conducting water chain in photosystem II. *J. Phys. Chem. Lett.* **2016**, *7*, 1925−1932.
(51) Smitienko, O. A.; Feldman, T. B.; Petrovskaya, L. E.; Nekrasova, O. V.; Yakovleva, M. A.; Shelaev, I. V.; Gostev, F. E.; Cherepanov, D. A.; Kolchugina, I. B.; Dolgikh, D. A.; Nadtochenko, V. A.; Kirpichnikov, M. P.; Ostrovsky, M. A. Comparative femtosecond spectroscopy of primary photoreactions of *Exiguobacterium sibiricum* rhodopsin and *Halobacterium salinarum* bacteriorhodopsin. *J. Phys. Chem. B* **2021**, *125*, 995−1008.

https://doi.org/10.1021/acs.biochem.4c00182
Biochemistry 2024, 63, 1505−1512